Neurobiology of Disease 146 (2020) 105131

Contents lists available at ScienceDirect

Neurobiology of Disease

journal homepage: www.elsevier.com/locate/ynbdi

The SARS-CoV-2 spike protein alters barrier function in 2D static and 3D microfluidic in-vitro models of the human blood–brain barrier

Tetyana P. Buzhdygan[a,b], Brandon J. DeOre[c], Abigail Baldwin-Leclair[c], Trent A. Bullock[a,b], Hannah M. McGary[a], Jana A. Khan[a], Roshanak Razmpour[a], Jonathan F. Hale[a], Peter A. Galie[c], Raghava Potula[a,b], Allison M. Andrews[a,b], Servio H. Ramirez[a,b,d,*]

[a] Department of Pathology and Laboratory Medicine, The Lewis Katz School of Medicine at Temple University, Philadelphia, PA 19140, United States of America
[b] Center for Substance Abuse Research, The Lewis Katz School of Medicine at Temple University, Philadelphia, PA 19140, United States of America
[c] Department of Biomedical Engineering, Rowan University, Glassboro, NJ 08028, United States of America
[d] The Shriners Hospitals Pediatric Research Center, Philadelphia, PA 19140, United States of America

ARTICLE INFO

Keywords:
COVID-19
SARS-CoV-2
Cerebral vascular biology
Blood-brain barrier
Neuroinflammation
Microfluidic chip
Tissue engineering

ABSTRACT

As researchers across the globe have focused their attention on understanding SARS-CoV-2, the picture that is emerging is that of a virus that has serious effects on the vasculature in multiple organ systems including the cerebral vasculature. Observed effects on the central nervous system include neurological symptoms (headache, nausea, dizziness), fatal microclot formation and in rare cases encephalitis. However, our understanding of how the virus causes these mild to severe neurological symptoms and how the cerebral vasculature is impacted remains unclear. Thus, the results presented in this report explored whether deleterious outcomes from the SARS-CoV-2 viral spike protein on primary human brain microvascular endothelial cells (hBMVECs) could be observed. The spike protein, which plays a key role in receptor recognition, is formed by the S1 subunit containing a receptor binding domain (RBD) and the S2 subunit. First, using postmortem brain tissue, we show that the angiotensin converting enzyme 2 or ACE2 (a known binding target for the SARS-CoV-2 spike protein), is ubiquitously expressed throughout various vessel calibers in the frontal cortex. Moreover, ACE2 expression was upregulated in cases of hypertension and dementia. ACE2 was also detectable in primary hBMVECs maintained under cell culture conditions. Analysis of cell viability revealed that neither the S1, S2 or a truncated form of the S1 containing only the RBD had minimal effects on hBMVEC viability within a 48 h exposure window. Introduction of spike proteins to *in vitro* models of the blood-brain barrier (BBB) showed significant changes to barrier properties. Key to our findings is the demonstration that S1 promotes loss of barrier integrity in an advanced 3D microfluidic model of the human BBB, a platform that more closely resembles the physiological conditions at this CNS interface. Evidence provided suggests that the SARS-CoV-2 spike proteins trigger a pro-inflammatory response on brain endothelial cells that may contribute to an altered state of BBB function. Together, these results are the first to show the direct impact that the SARS-CoV-2 spike protein could have on brain endothelial cells; thereby offering a plausible explanation for the neurological consequences seen in COVID-19 patients.

1. Introduction

Coronavirus disease 2019 (COVID-19) is a rapidly emerging public health crisis. Initially reported as a pneumonia of unknown origins in the Hubei Province of China, it is now known that this devastating disease is caused by the severe acute respiratory syndrome corona virus 2 or SARS-CoV-2. SARS-CoV-2 is a novel human β-coronavirus that shares high sequence homology with SARS-CoV(Lu et al., 2020; Coronaviridae Study Group of the International Committee on Taxonomy of, V., 2020). Infection is primarily transmitted by respiratory droplets and from human to human contact with a median incubation period of approximately 5 days(Lauer et al., 2020).

The clinical spectrum of COVID-19 varies from asymptomatic, mild to moderate self-limiting disease in the majority of cases(Huang et al., 2020; Hassan et al., 2020; Wang et al., 2020). However, severe and fatal consequences can occur in some patients with comorbidities such as

* Corresponding author at: Department of Pathology and Laboratory Medicine, Temple University Lewis Katz School of Medicine, 3500 N, Broad St. MERB 844, Philadelphia, PA 19140, United States of America.
E-mail address: servio@temple.edu (S.H. Ramirez).

https://doi.org/10.1016/j.nbd.2020.105131
Received 23 June 2020; Received in revised form 7 September 2020; Accepted 6 October 2020
Available online 11 October 2020

cardiovascular/pulmonary disease and diabetes(Guzik et al., 2020; Yang et al., 2020; Moriguchi et al., 2020). The most common symptomology in patients includes fever, dry cough, fatigue, diarrhea, alteration in taste/smell, conjunctivitis, and pneumonia(Lauer et al., 2020; Chan et al., 2020). Patients with severe respiratory infection can progress to acute respiratory distress syndrome (ARDS) and to multiple organ failure(Tay et al., 2020). Severity of disease in COVID-19 patients is associated with immune system dysregulation, such as lymphopenia and inflammatory cytokine storm. Among the other distinctive features of COVID-19 are elevated D-dimer, C-reactive protein, procalcitonin, LDH, ferritin, LFTs, and reduced CD4+/CD8+ T cells, which is predictive of mortality (Liu et al., 2020; Chen et al., 2020; Guan et al., 2020; Zhang et al., 2020).

The pulmonary system is principally involved in fatal COVID-19 cases. Histopathological observation from several autopsy studies have described diffuse alveolar damage with necrosis of alveolar lining cells, pronounced reactive type II pneumocytes, linear intraalveolar fibrin deposition and hyaline membrane formation consistent with diffuse alveolar damage(Martines et al., 2020; Buja et al., 2020). Additionally, evidence suggest broad tropism for SARS-CoV-2 in the kidneys, heart, large intestines, spleen, and liver(Bradley et al., 2004). Nevertheless, despite widespread interest in the pathophysiology of the disease, much remains unknown about how SARS-CoV-2 affects the CNS. Neurological signs, such as headache, nausea, vomiting and impaired consciousness have been reported(Carod-Artal, 2020; Pranata et al., 2020) with COVID-19 thus raising the plausibility that SARS-CoV-2 may neuroinvade the central nervous system (CNS). In fact, encephalitis has been observed in species such as feline(Rissi, 2018), porcine(Mora-Diaz et al., 2019) and murine(Roth-Cross et al., 2008) as a result of coronavirus neurotropism(Natoli et al., 2020). Additionally, SARS-CoV-1, the most closely related coronavirus to SARS-CoV-2, is known to infect the brain stem of both human and animals(Netland et al., 2008). Recently, a case of meningitis/encephalitis was first reported in a patient with COVID-19[24] supporting the prospect of neuroinvasion.

A key pathological mechanism of action for SARS-CoV-2 appears to involve the vasculature. One of the primary cellular targets for the virus to bind is the angiotensin converting enzyme 2 (ACE2)(Ou et al., 2020); a cell surface carboxypeptidase part of the renin-angiotensin system (RAS) that is responsible for a myriad of functions in the cardiovascular system. Specifically, ACE2 catalyzes the degradation of angiotensin II to angiotensin fragment (1–7) (Ang-(1–7)), which is associated with vasodilation and the subsequent decrease of hypertension(Mali et al., 2020; Santos, 2014). Of note, studies on COVID-19 patients indicate the presence of increased serum levels of angiotensin II[28]. ACE2 is expressed throughout the vasculature(Coronaviridae Study Group of the International Committee on Taxonomy of, V., 2020) of the body allowing SARS-CoV-2 access to multiple organ systems, as evidence of detection of virus-like particles in pulmonary(Ackermann et al., 2020) and the kidney(Varga et al., 2020) endothelium of COVID-19 patients. In regards, to the CNS, ACE2 is also expressed on the human cerebral vasculature(Kehoe et al., 2016; Bryce et al., 2005), which we also confirm herein. However, how the virus and its engagement of ACE2 potentially alters the blood-brain barrier (BBB) and contributes to the possible onset of neurological complications remains an open question.

The present study was aimed to identify whether the spike protein of the SARS-CoV-2 virus negatively affects the function of the BBB. To this end, we examined the effects of the following SARS-CoV-2 spike protein subunits on the status of the BBB: the receptor binding subunit S1 and the fusion subunit S2, as well as receptor binding domain (RBD) of the S1 subunit. As previously reported, we confirm that the primary cellular binding target of the S1 subunit, ACE2, is present in the human cerebral vasculature. Importantly, we also show for the first time that vascular ACE2 appears upregulated in brain tissue derived from cases of dementia and hypertension. To test functional outcomes, two (a 2D and a 3D vessel-like) in-vitro models of the BBB using primary brain endothelial cells were used. In both models, the effects of the spike subunits of SARS-CoV-2 on barrier integrity were determined. Our results provide evidence of endothelial barrier permeability and pro-inflammatory responses upon exposure to these subunits. Moreover, our analysis points to barrier breach that may be independent of ACE2 since deleterious effects also occurred with the S2 subunit. To the authors knowledge, this is the first evaluation for the effects of SARS-CoV-2 spike protein on the BBB.

2. Materials and methods

2.1. Reagents

SARS-CoV-2 subunit S1 (RayBiotech, Cat No 230–01101), SARS-CoV-2 RBD (RayBiotech, Cat No 230–01102), and SARS-CoV-2 subunit S2 (RayBiotech, Cat No 230–01103) derived from E.coli and SARS-CoV-2 S1 (RayBiotech, Cat No 230–30161-10), SARS-CoV-2 S2 derived from HEK293 cells were used in experiments where indicated. We used SARS-CoV-2 spike protein subunits concentrations ranging from 0.1 nM to 50 nM based on a previous study that tested the effects of SARS-CoV-2 protein on stimulating human immune cells(Dosch et al., 2009). Other recombinant proteins (i.e TNFα) were purchased from R&D Systems (Minneapolis, MN, USA). Note, recombinant proteins diluted to the concentrations used for these studies were assayed for the presence of E.coli endotoxin using the ToxinSensor Chromogenic LAL Endotoxin Assay (GenScript) which found E.coli endotoxin levels to be only at negligible amounts.

2.2. Endothelial cell culture

Primary human brain microvascular endothelial cells (hBMVECs) were isolated from fetal brain tissue as described(Andrews et al., 2018). Healthy tissue was provided (under informed consent) by the Laboratory of Developmental Biology (University of Washington, Seattle, WA) with approval granted by Temple University's (Philadelphia, PA) Institutional Review Board and in full compliance by the National Institutes of Health's (NIH) ethical guidelines. Cells were grown on rat tail collagen I coated flasks (BD Biosciences) in full growth medium (EBM-2 medium supplemented with EGM-2MV SingleQuots (Lonza, Cat No CC-3156 and CC-4147)) in an incubator set to 37 °C, 5% CO_2, and 100% humidity. Experiments were performed in the basal medium (EBM2 supplemented with 10% FBS).

For certain studies (as indicated in the figures), the hCMEC/D3 (a gift from Dr. Pierre O Couraud, Institut Cochin, université Paris Descartes, Paris, France) cell line that are often used for modeling the BBB were used. The cell line is a telomerase-immortalized human brain endothelial cell line for which its barrier forming properties and cell culture conditions have been previously characterized(Weksler et al., 2005).

2.3. 3D BBB model

Three-dimensional models of the blood-brain barrier (3D BBB) were fabricated by polymerizing hydrogels composed of 5 mg/mL type I collagen, 1 mg/mL hyaluronan, and 1 mg/mL Matrigel within microfabricated devices. The full method for this approach is described in a previous study(Partyka et al., 2017). Briefly, hydrogels were injected into the reservoir of the device and 180-μm needles coated in 0.1% BSA were inserted prior to polymerization to create two parallel and cylindrical voids within the gel. hCMEC/D3 were injected into one channel at a density of 10 million per mL (15 μL per channel). Channels were incubated for 10 min to ensure cell attachment then injected with cells again and inverted for 10 min to coat the opposing side to ensure full coverage. Following cell seeding, channels were exposed to 0.7 dyn/cm^2 of steady shear stress for four days using a linear syringe pump (Kent Scientific) to establish barrier function. Following the four-day perfusion, vessels were perfused for two hours with 50 nM of SARS-

CoV-2 subunit S1. Following exposure to the viral protein, vessels were either placed in fixative or prepared for permeability testing. To quantify localization of ZO-1 to the cell-cell junction in these vessels, the fluorescence intensities along representative 100-μm sections of both the control and spike protein-treated condition were plotted as described in a previous study(DeOre et al., 2019). The variance of both these intensity plots were calculated, and the percent difference was calculated to quantify the reduction in localization of ZO-1 to the cell-cell junctions.

2.4. Electric cell-substrate impedance sensing assay

Real-time changes of transendothelial electrical resistance (TEER) was measured using the ECIS ZTheta 96 Well Array Station (Applied Biophysics). ECIS was recorded using the multiple frequency/time (MFT) option to continuously monitor changes in impedance over spectrum of frequencies (400 Hz to 48,000 Hz). 96W20idf PET arrays were incubated with 10 mM cysteine solution to stabilize gold electrodes followed by coating with rat tail collagen type 1. Cells were plated at the density of 10,000 cells per each well with one well left cell-free for modeling purpose. Cells were grown until a confluent monolayer and functional barrier was formed as indicated by stable resistance > 600 Ohm at 4000 Hz and capacitance < 20 mA at frequency 48,000 Hz were reached. For the growing phase (5 to 7 days) cells were maintained in full growth medium with 50% of medium changed every second day. After confluency, medium was changed to the basal medium and SARS-CoV-2 subunit S1, SARS-CoV-2 subunit S2, or SARS-CoV-2 RBD at 0.1 nM, 1 nM or 10 nM concentrations were added to quadruplicated wells and recording continued for 48 h. Intercellular barrier resistance component was extracted using the Rb (barrier resistance) modeling function of the ECIS software (Applied Biophysics).

2.5. Permeability assays (2D)

To evaluate the paracellular permeability under static conditions, cells were seeded at the density of 10,000 cell per collagen I coated Transwel insert (pore size 0.4 μm, diameter 0.33 cm^2, Corning) in 200 μL of full growth medium. Basolateral chambers were filled with 500 μL of full growth medium. Medium was changed every 3 days. After confluent monolayer was formed, medium was changed to the basal medium and hBMVEC monolayers were incubated with 10 ng/mL TNF-α, or 10 nM SARS-CoV-2 subunit S1, SARS-CoV-2 subunit S2 or SARS-CoV-2 RBD for 24 h. 3 kDa FITC-DEAE-conjugated dextran (Sigma) was added to the apical chamber to the final concentration of 1 mg/mL and 1 h later, fluorescence in the basolateral chambers was determined using a SpectraMax M5e (Molecular Devices). Percent permeability was calculated as the relative fluorescence of medium in the spike protein-treated vs untreated cells.

2.6. Permeability assay (3D)

For permeability measurements, 3D vessels were transferred to the stage of an inverted epifluorescence microscope enclosed by an environmental chamber set to 37 ˚C, 5% CO_2, and 95% humidity. The channels were perfused with 4-kDa dextran-FITC at a flow rate of 5 μL/min using a syringe pump for 10 min, while submerged within culture medium to ensure cell viability. This flow rate was selected to assure fully developed flow throughout the channel and to maintain consistency with previous work. Images were taken at 30 s intervals for 10 min, and the diffusion coefficients were established using the following equation from previous work(Adamson et al., 1994).

$$P = \frac{dI}{dt}\frac{r}{2I_0}$$

where P is the permeability coefficient, dI/dt is the rate of change in fluorescence intensity outside the 3D vessel, r is the vessel radius, and I_0 is the fluorescence intensity inside the 3D vessel.

2.7. Cytotoxicity assay

The LIVE/DEAD viability/cytotoxicity assay (Life Technologies, Cat No L3224) was used to evaluate the toxicity of the SARS-CoV-2 spike protein to hBMVECs. Briefly, hBMVECs were seeded on a sterile 96-well plate at 1×10^4 cells per well and grown to confluency. Confluent cells were treated with 10 nM SARS-CoV subunit S1, SARS-CoV-2 subunit S2 or SARS-CoV-2 RBD for 48 h. 200 μL of 1 μM calcein-AM and 5 μM ethidium homodimer-1 were added to each well and incubated for 30 min at room temperature. Data was acquired at excitation and emission wavelengths of 495/515 nm for live cells and 528/617 nm for dead cells and normalized to the total number of cells.

2.8. Flow cytometry

Cells plated in 12-well dishes were grown to confluency and treated with 10 nM of SARS-CoV-2 subunit S1, SARS-CoV-2 subunit S2, SARS-CoV-2 RBD, or 100 ng/mL of TNF-α for 4 h or 24 h. After treatment, cells were washed with calcium and magnesium-free phosphate buffer saline (PBS) and detached with accutase for 1–2 min at 37 ˚C. Cells were then pelleted by centrifugation at 1000 rpm for 5 min and re-suspended in the Fixation Buffer (eBioscience/Thermo Fisher) for 30 min. Following fixation, cells were washed with Flow Cytometry Buffer (5% FBS, 0.1% sodium azide) and pelleted again. Cells were resuspended for 30 min in 100 μL of Flow Cytometry Buffer, containing 5 μL of anti-ICAM-1 (Pe-Cy7-conjugated, BioLegend, Cat No 356116) and 5 μL of anti-VCAM-1 (APC-conjugated, BioLegend, Cat No 305810) antibodies. Cells were then washed, pelleted and resuspended in Flow Cytometry Buffer for FACS analysis. 10,000 events per sample were acquired with a FACS BD Canto II flow cytometer (BD Biosciences) and data was then analyzed with FlowJo software.

2.9. Quantitative real time PCR

Confluent cell monolayers were treated with 10 nM SARS-CoV-2 subunit S1, SARS-CoV-2 subunit S2, or SARS-CoV-2 RBD for 24 h and briefly rinsed with PBS. To examine the concentration of mRNA, total RNA was extracted using TRIzol and PureLink RNA extraction reagents (Invitrogen). cDNA was synthesized with 400 ng of RNA in 20 μL reaction mix using High Capacity cDNA Reverse Transcriptase kit (Applied Biosystems). qRT-PCR was performed using TaqMan Universal 2× Master Mix (Thermo Scientific) and human *TIMP-1* (Hs01092512), *MMP2* (Hs01548727), *MMP3* (Hs00968305), *MMP9* (Hs00957562), *MMP12* (Hs00159178), *IL1β* (Hs01555410), *IL6* (Hs00174131), *CXCL10* (Hs00171042), *CCL5* (Hs00982282) FAM-labeled probes. *18S* rRNA (Cat No 4352930). was used as an internal control. Gene expression levels were analyzed using the $2^{-\Delta\Delta Ct}$ algorithm.

2.10. Protein electrophoresis and immunoblotting

Confluent cell monolayers were treated with 10 nM SARS-CoV-2 subunit S1, SARS-CoV-2 subunit S2, or SARS-CoV-2 RBD for 24 h and briefly rinsed with PBS. Whole cell lysate was prepared using RIPA buffer (EMD Milipore, Cat No 20–188) as per manufacturer's protocol. Obtained fractions were subjected to 10% Bis-Tris polyacrylamide gel electrophoresis in MOPS buffer under denaturing conditions and transferred to a 0.45 μm PVDF membrane. Membranes were blocked with Odyssey blocking buffer in Phosphate-buffered saline (Li-Cor Biosciences, Cat No 927–40000) for 1 h at room temperature. Blocked protein blots were incubated with affinity-purified rabbit anti-ACE2 (1:1000, Abcam, Cat No 15348), and mouse anti-β-Actin (1:5000, Sigma, Cat No A5441), in PBS supplemented with 0.05% Tween-20 and 10% Odyssey blocking buffer at 4 ˚C overnight, followed by incubation

with goat anti-rabbit IRDye 800CW IgG and goat anti-mouse IRDye 680RD secondary antibody in PBS (1:20,000) at room temperature for 1 h. Protein blots were visualized with Odyssey LiCor Imaging System. Band intensities were quantified using ImageJ software (NIH, Bethesda). Data is presented as relative intensity of ACE2 bands in S1, S2, or RBD-treated samples compared to the untreated samples and normalized to β-Actin.

2.11. Immunohistochemistry and imaging

Formalin-fixed paraffin-embedded human cortical tissue blocks of both normal ($N = 3$) and diseased origin (dementia, $N = 4$ cases and hypertension N = 4 cases) were procured from ProteoGenex, Inc. (Inglewood, CA), and serially sectioned at a thickness of 5 μm each. Donor ages ranged from 34 to 89 of both sexes. Donor information including comorbidities and cause of death are listed in supplemental table 1. For the dementia cases, donor 1–3 were classified as Alzheimer's Disease and donor 4 was mixed-type dementia. Glass slide-mounted sections were cleared, rehydrated and placed through heat-induced epitope retrieval (HIER) using Tris-EDTA buffer (pH 9.0) in preparation for immunohistochemical staining. HIER pre-treated sections were blocked for endogenous alkaline phosphatase activity and non-specific antibody binding using Bloxall (Vector Laboratories, SP-6000) and 2.5% Normal Horse Serum (Vector Laboratories, S-2012), respectively. The sections were subsequently incubated in rabbit anti-human ACE2 antibody (1:500, Abcam, ab15348) for 1 h at room temperature. Positive antibody binding was detected using anti-rabbit IgG ImmPRESS-AP polymer reagent (Vector Laboratories, MP-5401) and visualized via a 10 min incubation in Vector Blue AP substrate (Vector Laboratories, SK-5300). Stained sections were dehydrated, cleared and permanently mounted with VectaMount (Vector Laboratories, H-5000) for subsequent bright field imaging.

For Imaging, all sections were scanned with an EasyScan slide scanner (Motic Instruments Inc.). Images were examined in 2 mm × 2 mm regions of interest (ROIs) for expression of ACE2 on blood vessels (based on morphological appearance). Image analysis was performed with the NIS Elements AR (Nikon) imaging software using the measuring and line intensity profile tools. 50 capillary sized vessels (under 10 μm in diameter/caliber) for each ROI (3 per case) were examined as indicated above and the average and SEM calculated.

2.12. Statistical analysis

The experiments were independently performed multiple times (at least three times for all the data shown) to allow statistical analyses. Within each individual experimental set, primary cells from at least 3 donors were used, and every condition/per donor was evaluated in at least three replicates. One-way ANOVA with post-hoc Tukey's test was used to analyze difference between three of more groups with normal (Gaussian) distribution. One-way ANOVA with post-hoc Dunnett's test was utilized when multiple group comparisons were performed against a reference control. The Kruskal-Wallis test was used to analyze non-parametric distributed data sets (Fig. 1D and F). Results are expressed as the mean ± SEM with differences considered significant at $p < 0.05$. The data collected was analyzed using Prism v6.0 (GraphPad Software, San Diego, CA).

3. Results

3.1. ACE2 expression in human cerebral vasculature and in primary human brain endothelial cells (hBMVECs) in vitro

Previous reports on the structure and biochemical interactions of the SARS-CoV-2 spike protein with cellular protein targets have revealed that binding to the ACE2 membranous protein is a critical step for SARS-CoV-2 to enter target cells. Although the ACE-2 enzyme has been reported to be expressed in the cerebral vasculature(Kehoe et al., 2016; Hamming et al., 2004), little information is available regarding whether ACE2 is observed in capillary sized vessels and whether ACE2 levels are affected as a function of existing neuropathology. Thus, immunostaining for ACE2 was performed on postmortem brain tissues from normal cases lacking any detectable neuropathologies and from cases from patients that had a diagnosis of neurodegenerative disease (dementia) or a history of hypertension (see Table1 under supplemental information, for details on the demographic and clinical history of the cases evaluated). Dementia and hypertension were chosen since such underlying conditions are known to increase the severity of illness from COVID-19. As shown in Fig. 1, expression of ACE2 is clearly detected in the frontocortical regions of the brain. ACE2 appears in small vessels that form capillary networks (Fig. 1A, top left) and is also observed is larger caliber vessels (Fig. 1A, top left, bottom left and bottom right). Cross-sectioned vessels shows staining throughout the vessel wall and within the medial layers. Tissue sections from cases of dementia had a higher degree of ACE2 expression that was also found throughout the brain parenchyma in morphologically appearing astrocytes and in all types of vessel calibers (Fig. 1B). In cases of hypertension (Fig. 1C), ACE2 appeared to have the highest expression but without ACE2 immunoreactive parenchymal cells. Image analysis was performed on capillary vessels that measured under 10 μm in diameter since this is the primary site for BBB exchange. Image densitometry based on pixel intensity line profiles across capillary vessels revealed that when compared to the control, the dementia cases had an average of 3.5 ± 0.29 (mean ± SEM) fold increase in ACE2 expression and the hypertension cases indicated a 5.1 ± 0.32 (mean ± SEM) fold in ACE2 expression. The results demonstrate that the main target of the SARS-CoV-2 spike protein is expressed in the brain vasculature and it also appears to be upregulated in underlying health conditions known to worsen COVID-19 outcomes.

Before examining whether the SARS-CoV-2 protein affects the properties of the BBB, the expression status of ACE2 was determined. Currently there is no available information on whether ACE2 is expressed in cultured hBMVECs or the hCMEC/D3 cell line and whether exposure to SARS-CoV-2 spike proteins alters the ACE2 expression profile in these cells. Confluent monolayers of hBMVECs and hCMEC/D3 were treated with 10 nM SARS-CoV-2 subunit S1, or subunit S2 for 24 h and whole cell lysates were immunoblotted and probed against ACE2. To account for any effects due to glycosylation, both forms of SARS-CoV-2 spike proteins expressed in E.coli (non-glycosylated) and in the mammalian HEK293 cell line (glycosylated) were used. As seen in the Fig. 1E, ACE2 is expressed in whole cell lysates of both endothelial cell cultures tested. Furthermore, ACE2 protein expression was not significantly affected when the cells were exposed to the glycosylated (HEK293) or non-glycosylated (E.coli) subunit forms. For hBMVECs, densitometry analysis (Fig. 1F) of ACE2 normalized to β-Actin bands did not show any difference between the untreated control group (mean ± SEM) 0.98 ± 0.07 and any of the treatment groups (TNFα 1.28 ± 0.26; E.coli-expressed subunit S1 1.25 ± 0.22, E.coli-expressed subunit S2 1.09 ± 0.35, HEK293-expressed subunit S1 1.19 ± 0.37, HEK293-expressed subunit S2 1.20 ± 0.31). Similarly, for hCMEC/D3, no observable significant differences between ACE2 protein expression were noted in the untreated control group (0.93 ± 0.05) or any of the treatment groups (TNFα 1.30 ± 0.51; E.coli-expressed subunit S1 1.20 ± 0.68, E.coli-expressed subunit S2 1.00 ± 0.44, HEK293-expressed subunit S1 0.79 ± 0.17, HEK293-expressed subunit S2 1.20 ± 0.92). Results are expressed as mean ± SEM.

Thus, our results confirm previous findings of ACE2 expression in the brain(Hamming et al., 2004) and further demonstrate that vessels of all calibers express the protein. Furthermore, ACE2 levels were increased in the cerebral vasculature as a result of neurodegeneration or hypertension, which are two underlying conditions known to worsen COVID-19 outcomes. ACE2 expression was also evaluated in cells (i.e

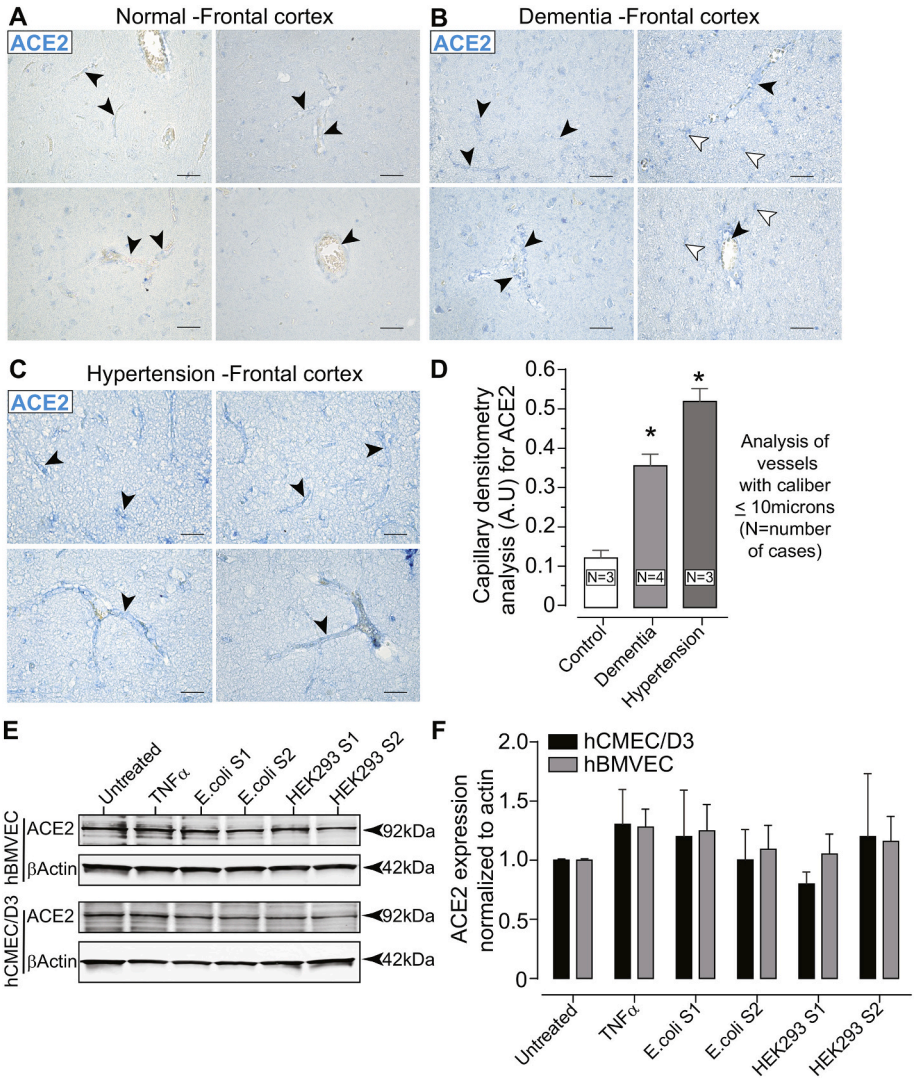

Fig. 1. ACE2 is expressed on the cerebral vasculature and in primary human brain microvascular endothelial cells (hBMVECs). Paraffin-embedded brain tissue was sectioned at 5 μm and immunostained for ACE2. Representative images of the frontal cortex from cases with no abnormal neuropathology (control) (A), dementia (B) and hypertension (C). The images were scanned at 40× objective magnification with ACE2 expression shown in blue (Vector Blue). Black arrow heads indicate the vascular presentation of ACE2 expression in various caliber vessels. White arrow heads point to ACE2 expression in parenchymal cells. Scalebars = 25 μm. (D) Bar graph of the quantification for ACE2 expression in capillary sized vessels (under 10 μm in diameter/caliber). (E) Western blots of hBMVECs and hCMEC/D3 cell lysates probed with ACE2 antibodies after cells were exposed to 10 nM of the SARS-CoV-2 subunit S1 or subunit S2 expressed either in E.coli or in HEK293 cells. (F) Bar graph of densitometry of the ACE2 immunoblot normalized to β-Actin. The experiment using hBMVECs was performed with three different donors and repeated three times. No significant differences between the groups were observed. (For interpretation of the references to colour in this figure legend, the reader is referred to the web version of this article.)

primary hBMVECs and hMEC/D3 cell cultures) that are typically used for modeling the BBB in-vitro. No change in ACE2 expression was noted as a function of spike protein subunit in the cell cultures tested.

3.2. SARS-CoV-2 spike protein does not affect brain endothelial cell viability

It is possible that the observed neurological effects of SARS-CoV-2 may be explained by the cytotoxicity induced by the spike protein. To date, no published information is available regarding whether SARS-CoV-2 spike protein impacts viability of human brain endothelial cells. Therefore, to assess the cell viability, hBMVECs were exposed to two different concentrations (1 nM and 10 nM) of SARS-CoV-2 subunit S1, subunit S2, or RBD for either 48 h or 72 h and analyzed using Live/Dead Cytotoxicity assay. The assay utilizes the combination of live cell-permeable acetomethoxy-derivative of calcein (calcein-AM) and live cell-impermeable ethidium homodimer-1 (EthD-1). The mild detergent, 0.1% saponin was used as a positive control to induce cell death. The data is represented as percent of cells that were fluorescent at 515 nm (calcein, live cells) or 617 nm (EthD-1, dead cells). The results in Fig. 2 show no evidence of cytotoxicity at 48 h with the concentrations tested. Values for live cells were as follows (mean ± SEM): untreated 99.85% ± 0.30%, saponin 39.35% ± 1.18% ($p < 0.05$), SARS-CoV-2 subunit S1 at 1 nM 99.78% ± 0.77% (ns) and at 10 nM 99.70% ± 0.49% (ns); SARS-CoV-2 RBD at 1 nM 99.49% ± 0.43% (ns) and at 10 nM 99.16% ± 0.27% (ns); SARS-CoV-2 subunit S2 at 1 nM 98.65% ± 0.36% (ns) and at 10 nM 98.30% ± 0.66% (ns). Values for dead cells were as follows mean ± SEM): untreated 0.15% ± 0.30% (ns), saponin 60.65% ± 1.18% ($p < 0.05$), SARS-CoV-2 subunit S1 at 1 nM S1 0.22% ± 0.77% (ns) and at 10 nM 0.30% ± 0.49% (ns); SARS-CoV-2 RBD at 1 nM 0.51% ± 0.43% (ns) and at 10 nM 0.84% ± 0.27% (ns); SARS-CoV-2 subunit S2 at 1 nM 1.35% ± 0.36% (ns) and at 10 nM 1.70% ± 0.66% (ns).

72 h of incubation with SARS-CoV-2 RBD and SARS-CoV-2 subunit S2 resulted in a slightly heightened rate of cell death. Values for live cells were as follows: untreated 100.08% ± 0.47%, saponin 26.00% ± 0.52% ($p < 0.05$), SARS-CoV-2 subunit S1 at 1 nM 98.83% ± 0.35% (ns) and at 10 nM 98.83% ± 0.35% (ns); SARS-CoV-2 RBD at 1 nM 95% ± 1.27% ($p < 0.05$) and at 10 nM 94.58% ± 0.74% ($p < 0.05$); SARS-CoV-2 subunit S2 at 1 nM 94.83% ± 0.69% ($p < 0.05$) and at 10 nM 98.58% ± 1.11% (ns). Values for dead cells were as follows: untreated 0.97% ± 0.38%, saponin 74.00% ± 0.54% ($p < 0.05$), SARS-CoV-2 subunit S1 at 1 nM 1.67% ± 0.35% (ns) and at 10 nM 1.67% ± 0.35% (ns); SARS-CoV-2 RBD at 1 nM 4.83% ± 1.27% ($p < 0.05$), and at 10 nM 5.42% ± 0.74% ($p < 0.05$); SARS-CoV-2 subunit S2 at 1 nM 5.17% ± 0.69% ($p < 0.05$) and at 10 nM 1.42% ± 1.11% (ns).

Overall, these findings indicate that the SARS-CoV-2 spike protein does not appear to affect brain endothelial cell viability after short-term exposure, suggesting that pathological effects on the endothelial barrier

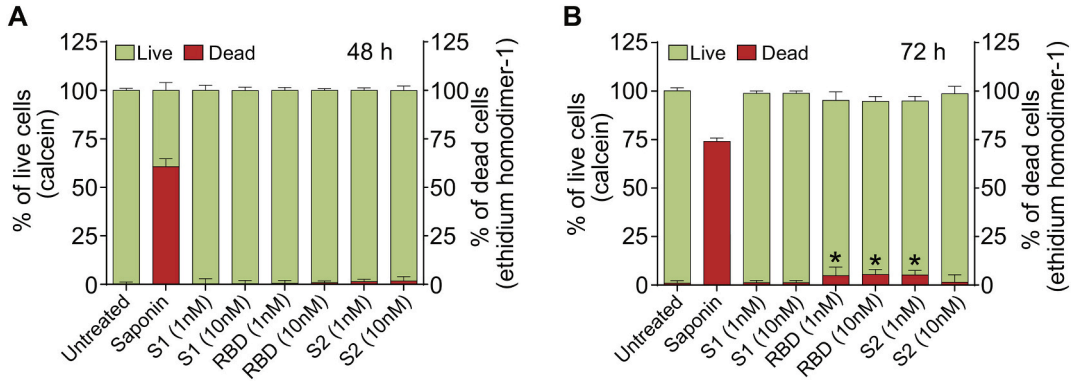

Fig. 2. SARS-CoV-2 spike protein does not affect brain endothelial cell viability. hBMVECs were treated with 1 nM and 10 nM of the SARS-CoV-2 subunit S1, SARS-CoV-2 RBD, and SARS-CoV-2 subunit S2 for 48 h (A) and 72 h (B). Cell viability was determined using the Live/Dead Cytotoxicity assay. Calcein positive (green) indicates live cells while ethidium homodimer-1 (EthD-1, red) indicates dead cells. Saponin was used a positive control. Data represents the ratio of live or dead cells in the total cell number and was obtained from two different donors, each performed in 6 replicates. Results are presented as mean ± SEM, $n = 12$, $^*p < 0.05$. p-values were computed using one-way ANOVA and Tukey post-hoc test. (For interpretation of the references to colour in this figure legend, the reader is referred to the web version of this article.)

properties reported in this work is unlikely attributed to a triggered cytotoxic effect.

3.3. SARS-CoV-2 spike protein induces loss of the BBB integrity

The main feature that distinguishes brain vascular endothelium from endothelium in the periphery is the abundant presence of tight junctions formed by adjacent cells. Tight junctions form the physical barrier of the BBB, preventing the free paracellular flux of ions and small molecules. We performed Electric Cell-Substrate Impedance (ECIS) study to determine whether changes to the barrier function are observed upon exposure to SARS-CoV-2 spike protein. This measure of electrical properties of the endothelial monolayer provides an analytical method to directly evaluate exogenous stimuli that may induce barrier "tightness" (higher resistance) or "leakiness" (lower resistance). ECIS measurements were acquired as described in Materials and Methods. The baseline resistance measured at 4000 Hz was 670, 590 and 780 Ohms for the 3 donors, respectively, and all resistance changes were calculated as a % change. As shown in Fig. 3A, the electrical resistance of the monolayers treated with the SARS-CoV-2 subunit S1 reached the lowest and plateaued at 8–12 h after the initial exposure (mean ± SEM): (−7.18% ± 2.64% ($p < 0.001$) for 10 nM, −3.79% ± 1.27% ($p < 0.001$) for 1 nM) followed by complete recovery in the case of 1 nM and 10 nM concentrations and continued decrease in the case of 0.1 nM concentration (down to −10.78% ± 3.52% ($p < 0.001$). In Fig. 3B, SARS-CoV-2 subunit S2 at 10 nM caused resistance to drop and plateau earlier (from 6 h to 14 h) with an average decrease of −7.56% ± 2.43% ($p < 0.001$) followed by recovery by 24 h. 1 nM and 0.1 nM concentrations of SARS-CoV-2 subunit S2 showed steady gradual decrease throughout whole experiment and reached maximum at 24 h (−6.29% ± 1.62% ($p < 0.001$) and − 6.54% ± 1.75% ($p < 0.001$). In the case of SARS-CoV-2 RBD (Fig. 3C), a dose-dependent drop of barrier occurred that reached maximum at 14 h post-exposure (−12.19% ± 2.74% ($p < 0.001$) for 10 nM, −8.42% ± 2.53% ($p < 0.001$) for 1 nM and − 5.4% ± 2.84% ($p < 0.001$) for 0.1 nM concentration).

To determine how the observed decrease in electrical resistance relates to the flux of molecules across the tight junctions, permeability assays were performed. To focus entirely on paracellular passage via the intercellular junctions we excluded transcytosis and transendothelial channels routes by using smaller molecular weight tracer bearing positive charge (3 k Da FITC-conjugated DEAE-dextran). As shown in Fig. 3D, at 1 h, 10 ng/mL TNFα (positive control) induced (mean ± SEM) 123.90% ± 5.60% (p < 0.001) permeability, 10 nM of SARS-CoV-2 subunit S1 induced 128.5% ± 4.11% ($p < 0.001$), 10 nM of SARS-CoV-2 subunit S2 resulted in 128.1% ± 4.25% ($p < 0.001$), and 10 nM of SARS-CoV-2 RBD showed no change at 113.3% ± 4.57% (ns). Additionally, the effects on permeability were not affected by the glycosylated status of the spike proteins (Supplemental Fig. 1).

Taken together, our data strongly suggest that the SARS-CoV-2 spike protein has the potency to cause a chronic low-grade dysfunction of the BBB that is a function of time and concentration. However, the observed leakage of the BBB cannot be exclusively attributed to the interaction of SARS-CoV-2 with its major cellular target ACE2, as effects induced by receptor binding domain (RBD), receptor binding subunit S1 and membrane fusing subunit S2 are all of comparable magnitude and temporal profile. Therefore, the likely explanation would be that SARS-CoV-2 executes its deleterious effect on the cerebral vasculature by engaging several cellular targets which most likely include pro-inflammatory cascades.

3.4. SARS-CoV-2 subunit S1 triggers increased BBB permeability in a 3D tissue engineered model of the BBB

In order to evaluate the effect of the SARS-CoV-2 spike protein on brain endothelial cells in an *in vitro* environment that mimics the three-dimensionality of the *in vivo* vasculature, barrier experiments were conducted using a 3D BBB model. The 3D BBB model was perfused for four days with 0.7 dyn/cm^2 of shear stress to assure formation of tight junctions necessary for barrier function (Fig. 4A-G). Following those four days, vessels were perfused for two hours with either 50 nM of SARS-CoV-2 subunit S1 or with cell culture medium. Both conditions were exposed to the same magnitude of fluid shear stress, 0.7 dyn/cm^2. Assessment of barrier permeability using 4 kDa FITC-dextran indicated a nearly three-fold increase in the permeability coefficient following exposure to the SARS-CoV-2 subunit S1 (Fig. 4F and G). Images of the vessels following dextran perfusion validated the permeability measurements; untreated vessels exhibited a sharp gradient of fluorescence at the vessel wall while treated vessels showed substantial leakage (Fig. 4F). Moreover, immunostaining for zonula-occludens-1 (ZO-1), a scaffolding protein in the tight junction complex, presented with reduced localization of ZO-1 to cell-cell junctions, which is indicative of barrier breakdown (Fig. 4D-E). Cell-cell junction localization was quantified by calculating the variance in fluorescence intensity of the ZO-1 stain over a 100-μm length of the vessel, which yielded a 38% reduction in the spike protein-treated condition compared to the control. Overall, these results support the findings of the 2D studies by demonstrating that the SARS-CoV-2 subunit S1 mediates barrier breakdown in a perfusable 3D configuration.

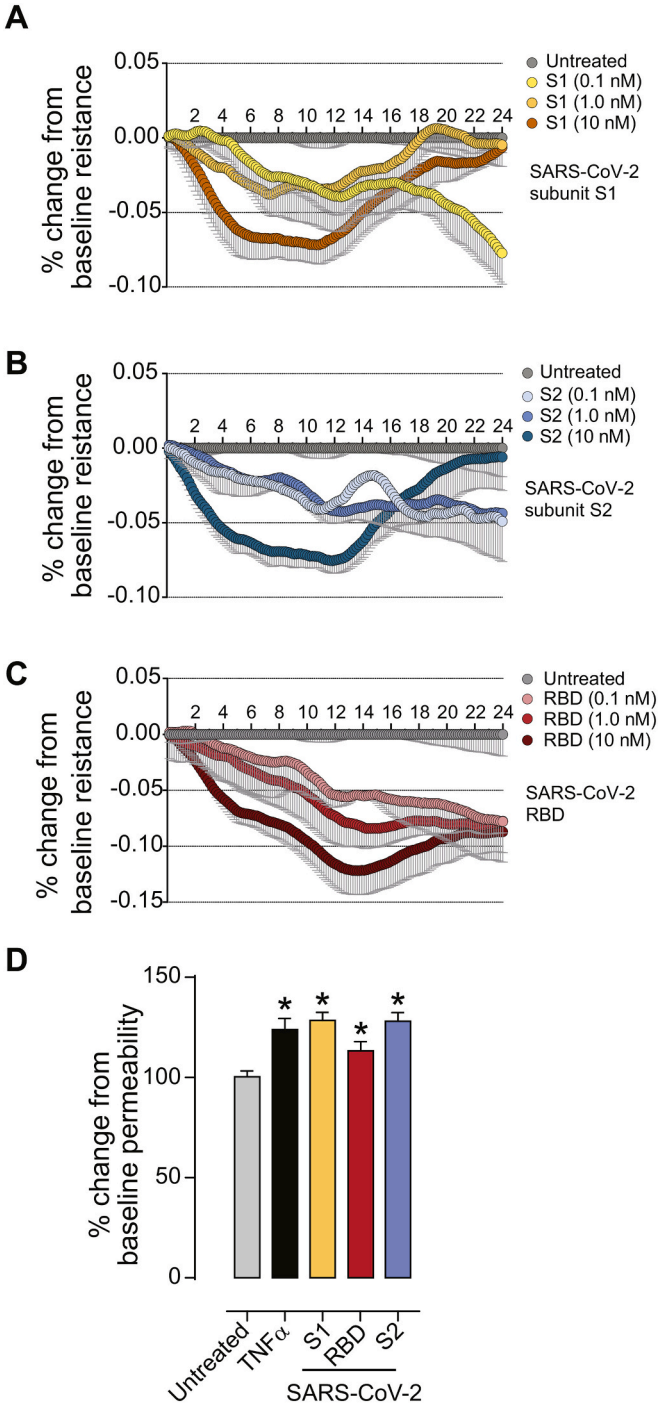

Fig. 3. SARS-CoV-2 spike protein compromises endothelial barrier properties. (A-C) Barrier electrical resistance was modelled based on continuous cell-substrate impedance readings recorded at 6 frequencies (400 Hz – 48 kHz) every 6 min for the duration of the time shown. Endothelial monolayers were treated with 0.1 nM, 1 nM or 10 nM of SARS-CoV-2 subunit S1, SARS-CoV-2 RBD, SARS-CoV-2 subunit S2 or left untreated to serve as a baseline. Treatments were initiated at 0 timepoint. The experiment was performed in quadruplicates and repeated three times using primary cells obtained from three different donors. Each data point is represented as the percentage of change from the baseline (mean ± SEM), $n = 12$. D. Barrier permeability to a small molecular tracer was determined 1 h after treatment using the 3 kDa FITC-conjugated DEAE-dextran. Endothelial monolayers were treated with 100 ng/mL TNF-α, 10 nM of SARS-CoV-2 subunit S1, SARS-CoV-2 RBD, SARS-CoV-2 subunit S2 or left untreated to serve as a baseline. The experiment was performed in quadruplicates and repeated three times using primary cells obtained from three different donors. Each data point is represented as mean ± SEM, n = 12, p-values were computed using one-way ANOVA and Tukey post-hoc test.

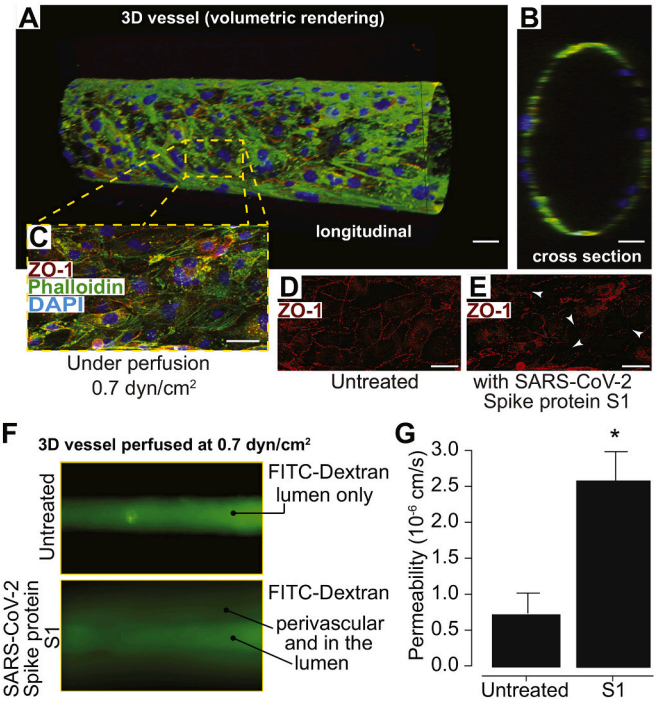

Fig. 4. SARS-CoV-2 subunit S1 alters barrier status in a 3D tissue engineered microfluidic model of the human BBB. Confocal microscopy and volumetric rendering were used to visualize the tissue engineered vessel. (A) Shows a longitudinal view of an endothelialized void after perfusion that formed a predictive vessel geometry analogous to those found within the brain. (B) provides a cross sectional perspective indicating a single layer of endothelial cells. In (C) a representative merged image of the engineered vessel constructs fixed and immunestained for the tight junction protein, ZO-1, along with phalloidin to label actin and the nuclear stain, DAPI. (D) shows the typical ZO-1 membranous pattern expected in mature barrier forming brain endothelial cells. (E) after perfusion for 2 h of SARS-CoV-2 subunit S1 (10 nM), constructs were also fixed and immunolabeled for ZO-1. The arrows point to areas in which the ZO-1 cellular pattern is discontinuous, punctate or absent signifying areas of barrier breach. Scalebar = 20 μm. (F) Fluorescence intensity after ten minutes of perfusion with 4 kDa FITC-dextran, indicating the impaired barrier function in vessels perfused after 2 h of the S1 spike protein versus untreated controls. G) Quantitative measurements for permeability coefficients of vessels exposed to the SARS-CoV-2 subunit S1 compared to untreated controls. Data was analyzed using Kruskal-Willis test, $n = 3$, $^*p < 0.05$.

3.5. The SARS-CoV-2 spike protein induces activation of brain endothelial cells

The experiments above showed that the SARS-CoV-2 spike protein significantly affects barrier integrity. It is possible that the viral spike protein triggers the activation and the pro-inflammatory response of the endothelial cells which results in barrier dysfunction. To test this possibility, flow cytometry experiments were performed to analyze the surface expression an of intracellular adhesion molecule-1 (ICAM-1) and vascular cell adhesion protein-1 (VCAM-1) expression as a function of time (4 h, 24 h). SARS-CoV-2 subunit S1, SARS-CoV-2 subunit S2, and SARS-CoV-2 RBD elicited a robust increase in ICAM-1 (Fig. 5A-C, E) and VCAM-1 (Fig. 5F-H, J) by 4 h and which remained elevated at 24 h. TNF-α was used as a control for endothelial activation (Fig. 5D, E, I, J). Baseline mean fluorescent intensity (MFI) was mean ± SEM 565.7 ± 19.1 for ICAM-1 and 394.0 ± 19.2 for VCAM-1. The SARS-CoV-2 subunit S1 elevated the MFI for ICAM-1 to 2279.0 ± 60.7 (4 h) and 2644.7 ± 93.1 at 24 h and represented a 4–4.5-fold increase (Fig. 5A, E). VCAM-1 was similarly affected and increased to MFI 1281.3 ± 28.5 (4 h) and 1572.7 ± 43.3 (24 h) (Fig. 5F, J). In the response to the SARS-CoV-2 RBD, ICAM-1 and VCAM-1 were also

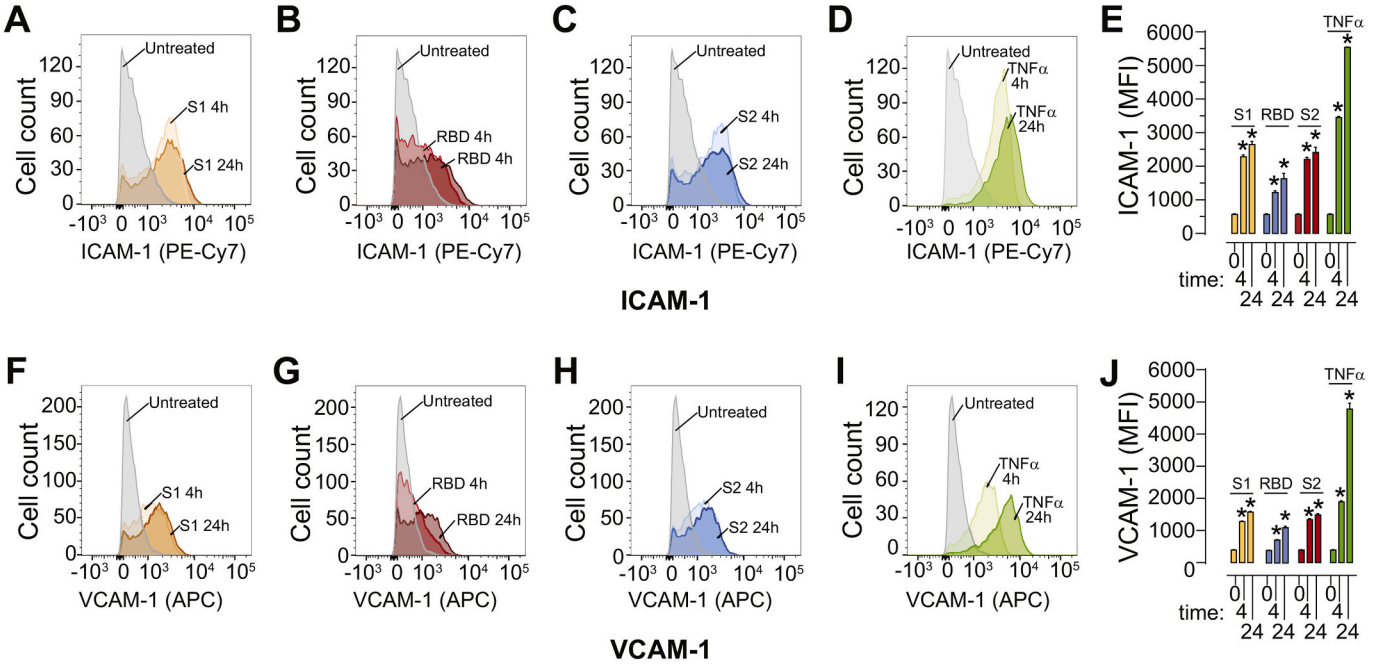

Fig. 5. SARS-CoV-2 spike protein triggers enhanced surface expression of adhesion molecules. Human brain microvascular endothelial cells (hBMVECs) were treated with 10 nM of SARS-CoV-2 subunit S1, SARS-CoV-2 RBD, SARS-CoV-2 subunit S2, or 100 ng/mL of TNF-α for 4 h or 24 h. Cells were stained for ICAM-1 and VCAM-1 expression and analyzed using a FACS Canto II flow cytometer. Shown are representative histograms for ICAM-1 expression in response to SARS-CoV-2 subunit S1 (A), SARS-CoV-2 RBD (B), SARS-CoV-2 subunit S2 (C), TNF-α (D) and the bar graph quantification of the Mean Fluorescent Intensity (MFI) (E). Representative histogram for VCAM-1 expression in response to SARS-CoV-2 subunit S1 (F), SARS-CoV-2 RBD (G), SARS-CoV-2 subunit S2 (H), TNF-α (I) and the bar graph quantification of MFI (J), $n = 3$, $^{*}p < 0.05$.

increased, albeit to a lesser degree. ICAM-1 MFI was 1223.0 ± 49.7 (4 h) and 1632.0 ± 160.1 (24 h) (Fig. 5B, E) while VCAM-1 MFI increased to 718 ± 28.1 (4 h) and 1101.3 ± 88.5 (24 h) (Fig. 5G, J). Finally, treatment with the SARS-CoV-2 subunit S2 induced a response similar to subunit S1 with ICAM-1 MFI increased to 2203.6 ± 61.3 at 4 h and 2409 ± 154.7 at 24 h (Fig. 5C, E); and VCAM-1 MFI increased to 1340.0 ± 56.7 at 4 h and 1487.3 ± 74.6 at 24 h (Fig. 5H, J). While the increase in ICAM-1 and VCAM-1 MFI was to a similar magnitude by 4 h for both the SARS-CoV-2 subunits S1 and S2 compared to TNF-α, the response to the spike proteins plateaued and did not increase further by 24 h unlike seen for TNF-α.

Together, these results provide evidence for the induction of a pro-inflammatory phenotype when hBMVECs are exposed to the SARS-COV-2 spike protein.

3.6. SARS-CoV-2 spike protein triggers a pro-inflammatory response and upregulation of matrix metalloproteinases in human brain endothelial cells

One possibility that could explain the destabilizing effects of the SARS-CoV-2 spike protein observed for the BBB function may be due to the endothelial pro-inflammatory response. We assessed gene expression of cytokines in cultured hBMVECs treated with the SARS-CoV-2 spike protein. As shown in Fig. 6A-B, IL-1β gene expression was significantly upregulated in the endothelial cells exposed to 10 nM SARS-CoV-2 RBD (mean ± SEM, at 4 h: 2.313 ± 1.05, $p < 0.001$) and SARS-CoV-2 subunit S1 (4 h: 2.378 ± 0.865, $p < 0.001$ and 24 h: 2.412 ± 0.317, $p < 0.001$). Similarly, IL-6 mRNA was significantly upregulated after 4 h of exposure to the SARS-CoV-2 subunit S1 (1.796 ± 0.533, $p = 0.014$), SARS-CoV-2 RBD (2.383 ± 1.311, $p < 0.001$), and SARS-CoV-2 subunit S2 (2.051 ± 0.449, $p < 0.001$). While 24 h treatment yielded significant results only for the subunit S1 (1.779 ± 0.702, $p = 0.017$). A marked significance in CCL5 gene expression was seen in all conditions tested and at both time points (subunit S1 at 4 h: 9.793 ± 7.151, $p < 0.0001$, and at 24 h: 13.99 ± 5.093, $p < 0.001$; RBD at 4 h: 6.181 ± 1.852, $p = 0.026$, and at 24 h: 6.344 ± 1.603, $p = 0.02$; subunit S2 at 4 h: 6.644 ± 4.352, $p = 0.01$ and at 24 h 8.529 ± 5.959, $p < 0.005$). CXCL10 mRNA was significantly upregulated in SARS-CoV-2 subunit S1-treated cells at 4 h (16.62 ± 7.33, $p < 0.001$) and at 24 h (5.251 ± 1.686, $p = 0.014$); and after 4 h of subunit S2 treatment (6.963 ± 4.409, $p < 0.001$). Although inflammatory responses by brain endothelial cells is counteractive to barrier stability, it is also possible that other cellular processes may contribute to the observed breach of the BBB. Another likely molecular target known to induce a compromise to the barrier integrity is the family of Matrix Metalloproteinases (MMPs). Thus, we examined the gene expression of MMPs specifically relevant to the BBB breakdown. As shown in Fig. 6C-D, 4 h of SARS-CoV-2 RBD exposure resulted in elevated expression (fold change ± SEM) of MMP2 (1.406 ± 0.076, $p = 0.012$), MMP3 (4.398 ± 0.223, $p = 0.003$), MMP9 (1.720 ± 0.140, $p < 0.005$), and MMP12 (3.271 ± 0.450, $p < 0.001$) in cultured hBMVECs. 24 h of SARS-CoV-2 RBD exposure resulted in elevated MMP2 (1.378 ± 0.134, $p < 0.022$), MMP3 (4.319 ± 0.437, $p = 0.0004$), MMP9 (1.66 ± 0.167, $p = 0.011$) and MMP12 (3.01 ± 0.177, $p < 0.001$) gene expression. SARS-CoV-2 subunit S1 exposure at 4 h affects only MMP3 (3.401 ± 0.304, $p = 0.016$) and MMP12 (3.416 ± 0.406, $p < 0.001$) gene expression. However, 24 h of subunit S1 exposure resulted in elevated MMP3 (5.557 ± 0.531, $p < 0.0001$), MMP9 (1.594 ± 0.254, $p = 0.027$), and MMP12 (3.305 ± 0.219, $p < 0.0001$). Similarly, SARS-CoV-2 subunit S2 at 4 h induced upregulation of MMP3 (7.849 ± 1.120, $p < 0.0001$) and MMP12 (3.021 ± 0.135, $p < 0.0001$), with unchanged MMP2 and MMP9. After 24 h of treatment with the SARS-CoV-2 subunit S2, MMP2 (1.613 ± 0.052, $p < 0.001$), MMP3 (3.520 ± 0.528, $p = 0.010$), MMP9 (1.705 ± 0.098, $p = 0.0058$), and MMP12 (4.076 ± 0.295, $p < 0.001$) were all significantly higher.

These analysis supports the notion that the SARS-CoV-2 spike protein can trigger a very specific pro-inflammatory response that includes upregulation of MMP expression in brain endothelial cells thereby offering a means for which SARS-CoV-2 may breach the BBB.

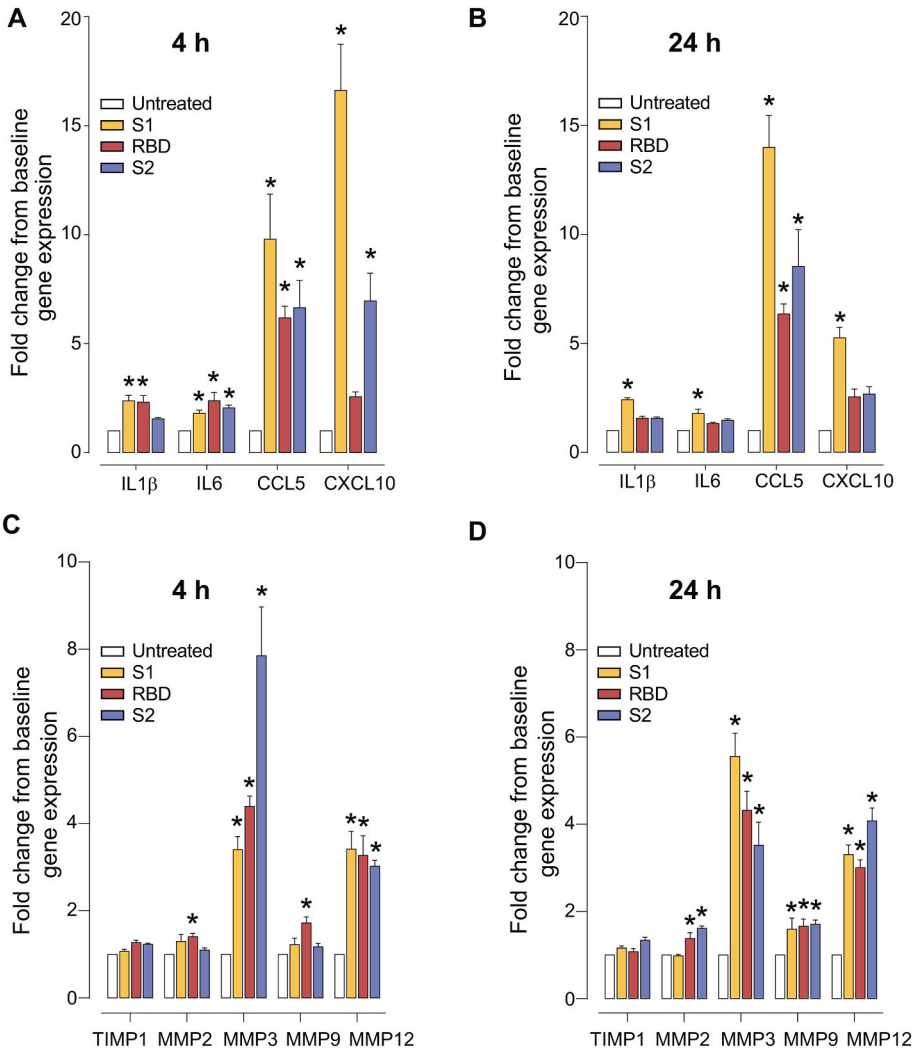

Fig. 6. SARS-CoV-2 spike protein triggers pro-inflammatory responses and upregulation of MMPs in hBMVECs. Confluent hBMVEC monolayers were incubated with 10 nM of SARS-CoV-2 subunit S1, SARS-CoV-2 RBD, SARS-CoV-2 subunit S2, for time indicated or left untreated to serve as a baseline control. Target cytokine genes analyzed included: IL1β, IL6, CCL5, CXCL10 at 4 h (A) and 24 h (B). Gene expression analysis for MMP2, MMP3, MMP9, MMP12 and the MMP inhibitor TIMP1 are shown for 4 h (C) and 24 h (D) respectively. Experiments were performed in quadruplicates and repeated three times using primary cells obtained from three different donors. Each bar represents a fold-change mean ± SEM, $n = 12$. Data sets were analyzed using one-way ANOVA and post-hoc comparison to the untreated condition were computed using Tukey post-hoc test with $^{*}p < 0.05$.

4. Discussion

The emergence of the COVID-19 pandemic and its ensuing consequences on public health has dramatically changed our way of life. Those with COVID-19 can be asymptomatic or present with a wide array of symptoms which critically influence recovery from the infection. The host's pro-inflammatory response, particularly in cases of aggressive inflammatory phenotypes, strongly contributes to disease prognosis. In severe cases, patients can progress to acute respiratory distress syndrome, septic shock, metabolic acidosis, coagulopathy and multiple organ dysfunction. COVID-19 patients are often present with neurological complications such as nausea, headache, anosmia, myalgia, impaired consciousness, and acute cerebrovascular diseases (Carod-Artal, 2020; Li et al., 2020; Koralnik and Tyler, 2020). The analysis within this report provides evidence that the SARS-CoV-2 spike protein can directly affect the barrier function of the BBB which gives deeper insight into the neuropathology associated with COVID-19.

SARS-CoV-2 can induce microclots formation in the vasculature of periphery tissues and within the vessels of the CNS. In fact, Bryce et al.[32] found that 6 out of 20 cases had microthrombi and acute infarction in the brain(Bryce et al., 2005). Here we report the evident breakdown of the BBB by SARS-CoV-2 spike protein, thus offering a possible avenue for counteracting the consequences of acute ischemic stroke observed in COVID-19 patients younger than 50 years old(Oxley et al., 2020). However, future studies should place focus on interrogating the connection between virus-mediated barrier disruption and coagulation to determine the unique cerebrovascular mechanisms responsible for heightening the risk of strokes in COVID-19 patients.

Angiotensin converting enzyme 2 or ACE2 is the primary cellular binding target for the SARS-CoV-2 spike protein. ACE2 expression or its enzymatic activity has been detected previously in the brain vasculature of healthy subjects, patients with neurodegenerative diseases, and in COVID-19 patients(Kehoe et al., 2016; Bryce et al., 2005; Hamming et al., 2004). Whether ACE2 expression is changed in patients with comorbidities (hypertension, diabetes etc.) remains unknown. Kehoe et al. recently reported reduced ACE2 activity in the brain tissue from patients with Alzheimer's disease (AD)(Kehoe et al., 2016). However, the abovementioned study did not provide a comparison of protein expression patterns in the AD vs control cases. Thus, our results make two important assertions by comparing normal cortex with cortex from dementia cases. The first is that ACE2 protein is found in different caliber vessels including capillaries, arterioles, and venules (Fig. 1). The second is that ACE2 expression appears upregulated in the capillaries of the dementia cases. Of note, our dementia cases included 3 with Alzheimer's and 1 mixed-type dementia. We also include an analysis of ACE2 in hypertension cases, which like dementia is also associated with poor COVID19 outcomes. Interestingly, the hypertensive cases showed even greater ACE2 expression in capillary sized vessels. ACE2 expression in parenchyma cells (ie. astrocytes, neurons etc.) was not evident in normal or hypertensive cases. In contrast, ACE2 immunopositive astrocytes were present in the dementia cases. In regards to ACE2 expression in other cell types associated with the cerebral vasculature, we

cannot discount the possibility of the contribution of ACE2 expression in pericytes and smooth muscle cells which has been reported by others (Hamming et al., 2004; He et al., 2005). Overall, dementia and hypertension clearly upregulates ACE2 vasculature expression which suggests that SARS-CoV-2 could have a higher probability to encounter its key cellular binding target in individuals with these comorbidities.

It is now well accepted that COVID-19 can strike all age groups, including children. An observed complication of SARS-CoV-2 infection in children is similar to atypical Kawasaki disease shock syndrome characterized by multisystemic hyperinflammation, edema, and vasculitis(Riphagen et al., 2020). Recent study attributes vascular and endothelial derangements found in COVID-19 patients to the direct viral infection of endothelial cells(Varga et al., 2020). In our study we showed that even SARS-CoV-2 spike protein alone is a potent inductor of endothelial dysfunction and that manifestations of COVID-19 shock syndrome in children can be at least partially attributed to its action. Thus, the clinically observed edema results from the hyperpermeable endothelial barrier and generalized diffused hyperinflammation can be caused by the elevated secretion of pro-inflammatory cytokines in endothelium. These findings provide two important notions for therapeutic interventions: 1) to stabilize the endothelium in COVID-19 patients with pre-existing conditions associated with heightened vulnerability of the vascular bed; and 2) productive viral infection of endothelial cells is not an absolute requirement for endothelial dysfunction, as it also can arrive as a result of viral protein shedding.

The BBB endothelial bed is the primary locus of attack for various neuroinvasive viruses including rabies(Wang et al., 2013; Chai et al., 2014), HIV-1(Marshall, 1988; Resnick et al., 1988; Berger and Avison, 2004), West Nile(Diamond and Klein, 2004; Paterson, 2005), Zika(Leda et al., 2019), and influenza(Chaves et al., 2014). Viral pathogens exert their negative affect on the BBB not only by the direct interaction with the endothelium that results in productive or nonproductive infection of endothelial cells, but also by the initiation of host immune responses and elevated expression of pro-inflammatory cytokines, chemokines, cell adhesion molecules, ultimately leading to a demise in the structural and functional integrity of the BBB[54]. Disruption of the BBB unleashes free passage of viral particles and infected immune cells into the brain parenchyma, further elevates levels of inflammatory mediators and aggravates the breach in the endothelial barrier function (Dahm et al., 2016; Spindler and Hsu, 2012; Daniels et al., 2014; Al-Obaidi et al., 2018). During the course of many systemic viral infections, shed viral proteins are potent inductors of BBB dysfunction thus we evaluated the effect of the essential SARS-CoV-2 spike protein on brain endothelial cells. We examined the cytotoxic effect of SARS-CoV-2 spike protein on endothelial cells and found that only chronic exposure ($>$ 72 h) of SARS-CoV-2 spike protein result in slightly increased rate of cell death. These findings extend recent clinical data that report endothelial cell death in severe case of COVID-19 (Varga et al., 2020). However, we cannot exclude the possibility that other cells that form and maintain the vascular bed (pericytes, perivascular immune cells, parenchymal cells etc) are susceptible to the SARS-CoV-2 spike protein cytotoxicity.

Next, we evaluated the SARS-CoV-2 spike protein for its ability to modulate endothelial barrier function. To evaluate the barrier integrity, we measured the electrical resistance (an analytical means to examine barrier “tightness”) and paracellular permeability (barrier “leakiness”) of hBMVECs exposed to either subunit of SARS-CoV-2 spike protein. Even single application of the spike protein subunits resulted in a dose-dependent loss of the barrier electrical resistance that peaked at 12–14 h. Interestingly, SARS-CoV-2 subunit S1 or S2 both caused similar effects and transient loss of electrical resistance that was completely recovered by 24 h, raising the possibility that structural reorganization rather than outright loss of tight junctional complex occurs (Fig. 3A and B). To determine whether the decrease in transendothelial resistance by the spike proteins corresponds to the leaky barrier, we performed a FITC-permeability assay. The results show that each subunit of SARS-CoV-2 spike protein significantly increases the rate of passive paracellular passage of small molecular tracers providing a second indicator of barrier dysfunction (Fig. 3D). The observation that subunits S1, S2 and RBD exert similar deleterious effects on the BBB function is particularly interesting as it strongly suggests that the ACE2 receptor is not the exclusive point of contact between SARS-CoV-2 and brain endothelial cells. Most likely the interaction between SARS-CoV-2 and the BBB is multifocal and involves reversible activation at more than one receptor or signaling cascade.

Endothelial cells are constantly exposed to fluid shear stress from the blood. Therefore, it is important to validate findings from static systems in BBB models that factor physiologic parameters such as dynamic flow and intercellular geometries. To this end, we performed experiments using brain endothelial cells grown in a cylindrical space within a gel matrix as described previously(Partyka et al., 2017). After endothelialization, perfusion was introduced to promote barrier genesis that generates properties featured at the BBB. In Fig. 4 these vascular constructs are shown to mature as a single layer (cross section) of endothelium that form intercellular tight junctions and restrict movement of fluorescent tracers. These systems (when also coupled with other cells) represent the most advanced recapitulation of the blood-brain barrier. Once the SARS-CoV-2 subunit S1 was introduced, the presence of barrier permeability (from lumen to parenchymal compartment) was clearly evident as early as 2 h. These results suggest that whether free viral spike proteins or those on the surface of the virus present during SARS-CoV-2 infection could induce barrier permeability (albeit once a certain threshold is reached) equivocal to the concentrations used here. As this is the first report on the topic, much work remains, particularly in regard to how permeability dynamics may change once these 3D microfluidic constructs are used with the whole SARS-CoV-2 virus.

Endothelial cells are an essential part of the inflammatory response since activation of the endothelium allows for recruitment and mobilization of immune cells to the tissues that are under pathogen attack. Once activated, brain endothelial cells upregulate expression of cell adhesion molecules (CAMs) and pro-inflammatory cytokines that play a key initial role in the process of neuroinflammation and transendothelial migration of immune cells in response to inflammatory challenge(Hurwitz et al., 1994; Roe et al., 2014). Endothelial cells exposed to the each subunit of the SARS-CoV-2 spike protein showed elevated expression of the cell adhesion molecules (ICAM-1 and VCAM-1, Fig. 5), leukocyte chemotaxis factors (CXCL10 and CCL5 (RANTES) Fig. 6), and pro-inflammatory cytokines (IL-1β and IL-6, Fig. 6). In conjunction with reduced barrier tightness (Fig. 2) our finding that SARS-CoV-2 activates hBMVECs strongly indicates the potential for enhanced immune infiltration into the CNS.

Endothelial activation also features increased expression of matrix metalloproteinase or MMPs, a family of enzymes involved in the remodeling of extracellular matrix in both normal physiological and pathological processes. Activated by pro-inflammatory cytokines (Daneman and Prat, 2015), MMPs also regulate tight junction protein degradation and post-translational modifications(Louboutin et al., 2010; Yang and Rosenberg, 2015; Roe et al., 2012). In this study, we report that the spike protein increases MMP3 and MMP12, and to a lesser extent MMP2 and MMP9 gene expression. MMP3 has been previously implicated in traumatic brain injury(Falo et al., 2006) by digesting tight junctions proteins followed by the BBB opening(Yang and Rosenberg, 2011). These reports corroborate our findings of decreased barrier resistance (Fig. 3) and heightened secretion of chemotactic chemokines (Fig. 5). MMP12, on the contrary, is not involved in BBB damage, but plays role in immune cells extravasation and migration into the brain(Ulrich et al., 2006). Taking together our data of elevated MMP3, CCL5, CXCL10 and CAMs, we can speculate that SARS-CoV-2 is a potentially neuroinvasive virus as it turns on the machinery to facilitate the migration of infected immune cells as “Trojan horses” into the brain parenchyma.

To our knowledge, this is the first reported evaluation that examined the effects of the SARS-CoV-2 spike protein on the BBB. Our

findings provide insight into the continued theme that this novel coronavirus triggers responses at the endothelium. Specifically, in regard to the brain endothelium, the SARS-CoV-2 spike protein induced destabilization of the BBB, promoted a pro-inflammatory status but did not appear to alter cell viability acutely. Dysfunction of the barrier offers a plausible explanation to the observed neurological complications seen in COVID-19. Lastly, the opening of the BBB, hints at the possible means in which the SARS-CoV-2 pathogen could also neuroinvade.

Supplementary data to this article can be found online at https://doi.org/10.1016/j.nbd.2020.105131.

Authors' contributions

TPB, SHR, RP, PAG, and AMA co-wrote the manuscript and designed experiments. TPB, AMA, ABL, TAB, HMM, JAK, RR performed experiments and analyzed the results. All authors have read and approved the manuscript.

Funding

Methodologies and reagents used were developed in part by the following funding sources: T32 DA007237 (TPB), 5R01DA046833 (SHR & RP) and K01DA046308 (AMA).

Availability of data and materials

The results of the analyzed data presented in this study are all included herein.

Ethics approval

The studies in this report were conducted under approval by Temple University's (Philadelphia, PA) Institutional Review Board and in full compliance by the National Institutes of Health's (NIH) ethical guidelines.

Declaration of Competing Interest

The authors declare no competing interests.

Acknowledgements

Human fetal tissue for the isolation of human fetal brain microvascular endothelial cells was obtained from the Birth Defects Research Laboratory which is supported by NIH award number 5R24HD000836 from the Eunice Kennedy Shriver National Institute of Child Health and Human Development. We would like to recognize the Temple University IBC committee (particularly program coordinator, Mary B. Pultro) for their attentive and efficient review which allowed these experiments to be performed in a timely manner.

References

Ackermann, M., et al., 2020. Pulmonary vascular Endothelialitis, thrombosis, and angiogenesis in Covid-19. N. Engl. J. Med. https://doi.org/10.1056/NEJMoa2015432.

Adamson, R.H., Lenz, J.F., Curry, F.E., 1994. Quantitative laser scanning confocal microscopy on single capillaries: permeability measurement. Microcirculation 1, 251–265. https://doi.org/10.3109/10739689409146752.

Al-Obaidi, M.M.J., et al., 2018. Disruption of the blood brain barrier is vital property of neurotropic viral infection of the central nervous system. Acta Virol. 62, 16–27. https://doi.org/10.4149/av_2018_102.

Andrews, A.M., et al., 2018. Characterization of human fetal brain endothelial cells reveals barrier properties suitable for in vitro modeling of the BBB with syngenic cocultures. J. Cereb. Blood Flow Metab. 38, 888–903. https://doi.org/10.1177/0271678X17708690.

Berger, J.R., Avison, M., 2004. The blood brain barrier in HIV infection. Front. Biosci. 9, 2680–2685. https://doi.org/10.2741/1427.

Bradley, B.T., et al., 2004. Histopathology and ultrastructural findings of fatal COVID-19 Infections. medRxiv 2020https://doi.org/10.1101/2020.04.17.20058545(2020). 2017.20058545.

Bryce, C., et al., 2005. Pathophysiology of SARS-CoV-2: targeting of endothelial cells renders a complex disease with thrombotic microangiopathy and aberrant immune response. The Mount Sinai COVID-19 autopsy experience. medRxiv 2020https://doi.org/10.1101/2020.05.18.20099960(2020). 2018.20099960.

Buja, L.M., et al., 2020. The emerging spectrum of cardiopulmonary pathology of the coronavirus disease 2019 (COVID-19): report of 3 autopsies from Houston, Texas, and review of autopsy findings from other United States cities. Cardiovasc. Pathol. 48, 107233. https://doi.org/10.1016/j.carpath.2020.107233.

Carod-Artal, F.J., 2020. Neurological complications of coronavirus and COVID-19. Rev. Neurol. 70, 311–322. https://doi.org/10.33588/rn.7009.2020179.

Chai, Q., He, W.Q., Zhou, M., Lu, H., Fu, Z.F., 2014. Enhancement of blood-brain barrier permeability and reduction of tight junction protein expression are modulated by chemokines/cytokines induced by rabies virus infection. J. Virol. 88, 4698–4710. https://doi.org/10.1128/JVI.03149-13.

Chan, J.F., et al., 2020. A familial cluster of pneumonia associated with the 2019 novel coronavirus indicating person-to-person transmission: a study of a family cluster. Lancet 395, 514–523. https://doi.org/10.1016/S0140-6736(20)30154-9.

Chaves, A.J., et al., 2014. Neuroinvasion of the highly pathogenic influenza virus H7N1 is caused by disruption of the blood brain barrier in an avian model. PLoS One 9, e115138. https://doi.org/10.1371/journal.pone.0115138.

Chen, G., et al., 2020. Clinical and immunological features of severe and moderate coronavirus disease 2019. J. Clin. Invest. 130, 2620–2629. https://doi.org/10.1172/JCI137244.

Coronaviridae Study Group of the International Committee on Taxonomy of, V, 2020. The species severe acute respiratory syndrome-related coronavirus: classifying 2019-nCoV and naming it SARS-CoV-2. Nat. Microbiol. 5, 536–544. https://doi.org/10.1038/s41564-020-0695-z.

Dahm, T., Rudolph, H., Schwerk, C., Schroten, H., Tenenbaum, T., 2016. Neuroinvasion and inflammation *in viral* central nervous system infections. Mediat. Inflamm., 8562805. https://doi.org/10.1155/2016/8562805(2016).

Daneman, R., Prat, A., 2015. The blood-brain barrier. Cold Spring Harb. Perspect. Biol. 7, a020412. https://doi.org/10.1101/cshperspect.a020412.

Daniels, B.P., et al., 2014. Viral pathogen-associated molecular patterns regulate blood-brain barrier integrity via competing innate cytokine signals. mBio 5https://doi.org/10.1128/mBio.01476-14. e01476-01414.

DeOre, B.J., Galie, P.A., Sehgal, C.M., 2019. Fluid flow rate dictates the efficacy of low-intensity anti-vascular ultrasound therapy in a microfluidic model. Microcirculation 26, e12576. https://doi.org/10.1111/micc.12576.

Diamond, M.S., Klein, R.S., 2004. West Nile virus: crossing the blood-brain barrier. Nat. Med. 10, 1294–1295. https://doi.org/10.1038/nm1204-1294.

Dosch, S.F., Mahajan, S.D., Collins, A.R., 2009. SARS coronavirus spike protein-induced innate immune response occurs via activation of the NF-kappaB pathway in human monocyte macrophages *in vitro*. Virus Res. 142, 19–27. https://doi.org/10.1016/j.virusres.2009.01.005.

Falo, M.C., Fillmore, H.L., Reeves, T.M., Phillips, L.L., 2006. Matrix metalloproteinase-3 expression profile differentiates adaptive and maladaptive synaptic plasticity induced by traumatic brain injury. J. Neurosci. Res. 84, 768–781. https://doi.org/10.1002/jnr.20986.

Guan, W.J., et al., 2020. Clinical characteristics of coronavirus disease 2019 in China. N. Engl. J. Med. 382, 1708–1720. https://doi.org/10.1056/NEJMoa2002032.

Guzik, T.J., et al., 2020. COVID-19 and the cardiovascular system: implications for risk assessment, diagnosis, and treatment options. Cardiovasc. Res. https://doi.org/10.1093/cvr/cvaa106.

Hamming, I., et al., 2004. Tissue distribution of ACE2 protein, the functional receptor for SARS coronavirus. A first step in understanding SARS pathogenesis. J. Pathol. 203, 631–637. https://doi.org/10.1002/path.1570.

Hassan, S.A., Sheikh, F.N., Jamal, S., Ezeh, J.K., Akhtar, A., 2020. Coronavirus (COVID-19): a review of clinical features, diagnosis, and treatment. Cureus 12, e7355. https://doi.org/10.7759/cureus.7355.

He, L., et al., 2005. Pericyte-specific vascular expression of SARS-CoV-2 receptor ACE2 – implications for microvascular inflammation and hypercoagulopathy in COVID-19. bioRxiv 2020https://doi.org/10.1101/2020.05.11.088500(2020). 2011.088500.

Huang, C., et al., 2020. Clinical features of patients infected with 2019 novel coronavirus in Wuhan, China. Lancet 395, 497–506. https://doi.org/10.1016/S0140-6736(20)30183-5.

Hurwitz, A.A., Berman, J.W., Lyman, W.D., 1994. The role of the blood-brain barrier in HIV infection of the central nervous system. Adv. Neuroimmunol. 4, 249–256. https://doi.org/10.1016/s0960-5428(06)80263-9.

Kehoe, P.G., Wong, S., Al Mulhim, N., Palmer, L.E., Miners, J.S., 2016. Angiotensin-converting enzyme 2 is reduced in Alzheimer's disease in association with increasing amyloid-beta and tau pathology. Alzheimers Res. Ther. 8, 50. https://doi.org/10.1186/s13195-016-0217-7.

Koralnik, I.J., Tyler, K.L., 2020. COVID-19: a global threat to the nervous system. Ann. Neurol. https://doi.org/10.1002/ana.25807.

Lauer, S.A., et al., 2020. The incubation period of coronavirus disease 2019 (COVID-19) from publicly reported confirmed cases: estimation and application. Ann. Intern. Med. 172, 577–582. https://doi.org/10.7326/M20-0504.

Leda, A.R., et al., 2019. Selective disruption of the blood-brain barrier by Zika virus. Front. Microbiol. 10, 2158. https://doi.org/10.3389/fmicb.2019.02158.

Li, H., Xue, Q., Xu, X., 2020. Involvement of the nervous system in SARS-CoV-2 infection. Neurotox. Res. 38, 1–7. https://doi.org/10.1007/s12640-020-00219-8.

Liu, Y., et al., 2020. Clinical and biochemical indexes from 2019-nCoV infected patients linked to viral loads and lung injury. Sci. China Life Sci. 63, 364–374. https://doi.org/10.1007/s11427-020-1643-8.

Louboutin, J.P., Agrawal, L., Reyes, B.A., Van Bockstaele, E.J., Strayer, D.S., 2010. HIV-1 gp120-induced injury to the blood-brain barrier: role of metalloproteinases 2 and 9 and relationship to oxidative stress. J. Neuropathol. Exp. Neurol. 69, 801–816. https://doi.org/10.1097/NEN.0b013e3181e8c96f.

Lu, R., et al., 2020. Genomic characterisation and epidemiology of 2019 novel coronavirus: implications for virus origins and receptor binding. Lancet 395, 565–574. https://doi.org/10.1016/S0140-6736(20)30251-8.

Mali, S.N., Thorat, B.R., Chopade, A.R., 2020. A viewpoint on angiotensin-converting enzyme 2, anti-Hypertensives and coronavirus disease 2019 (COVID-19). Infect Disord. Drug Targets. https://doi.org/10.2174/1871526520666200511005546.

Marshall, D.W., 1988. HIV penetration of the BBB. Neurology 38, 1000–1001. https://doi.org/10.1212/wnl.38.6.1000-b.

Martines, R.B., et al., 2020. Pathology and pathogenesis of SARS-CoV-2 associated with fatal coronavirus disease, United States. Emerg. Infect. Dis. 26. https://doi.org/10.3201/eid2609.202095.

Mora-Diaz, J.C., Pineyro, P.E., Houston, E., Zimmerman, J., Gimenez-Lirola, L.G., 2019. Porcine Hemagglutinating encephalomyelitis virus: a review. Front Vet. Sci. 6, 53. https://doi.org/10.3389/fvets.2019.00053.

Moriguchi, T., et al., 2020. A first case of meningitis/encephalitis associated with SARS-Coronavirus-2. Int. J. Infect. Dis. 94, 55–58. https://doi.org/10.1016/j.ijid.2020.03.062.

Natoli, S., Oliveira, V., Calabresi, P., Maia, L.F., Pisani, A. Does, 2020. SARS-Cov-2 invade the brain? Translational lessons from animal models. Eur. J. Neurol. https://doi.org/10.1111/ene.14277.

Netland, J., Meyerholz, D.K., Moore, S., Cassell, M., Perlman, S., 2008. Severe acute respiratory syndrome coronavirus infection causes neuronal death in the absence of encephalitis in mice transgenic for human ACE2. J. Virol. 82, 7264–7275. https://doi.org/10.1128/JVI.00737-08.

Ou, X., et al., 2020. Characterization of spike glycoprotein of SARS-CoV-2 on virus entry and its immune cross-reactivity with SARS-CoV. Nat. Commun. 11, 1620. https://doi.org/10.1038/s41467-020-15562-9.

Oxley, T.J., et al., 2020. Large-vessel stroke as a presenting feature of Covid-19 in the young. N. Engl. J. Med. 382, e60. https://doi.org/10.1056/NEJMc2009787.

Partyka, P.P., et al., 2017. Mechanical stress regulates transport in a compliant 3D model of the blood-brain barrier. Biomaterials 115, 30–39. https://doi.org/10.1016/j.biomaterials.2016.11.012.

Paterson, R., 2005. How West Nile virus crosses the blood-brain barrier. Lancet Neurol. 4, 18. https://doi.org/10.1016/s1474-4422(04)00957-3.

Pranata, R., Huang, I., Lim, M.A., Wahjoepramono, P.E.J., July, J., 2020. Impact of cerebrovascular and cardiovascular diseases on mortality and severity of COVID-19 - systematic review, meta-analysis, and meta-regression. J. Stroke Cerebrovasc. Dis., 104949. https://doi.org/10.1016/j.jstrokecerebrovasdis.2020.104949.

Resnick, L., Berger, J.R., Shapshak, P., Tourtellotte, W.W., 1988. Early penetration of the blood-brain-barrier by HIV. Neurology 38, 9–14. https://doi.org/10.1212/wnl.38.1.9.

Riphagen, S., Gomez, X., Gonzalez-Martinez, C., Wilkinson, N., Theocharis, P., 2020. Hyperinflammatory shock in children during COVID-19 pandemic. Lancet 395, 1607–1608. https://doi.org/10.1016/S0140-6736(20)31094-1.

Rissi, D.R., 2018. A retrospective study of the neuropathology and diagnosis of naturally occurring feline infectious peritonitis. J. Vet. Diagn. Investig. 30, 392–399. https://doi.org/10.1177/1040638718755833.

Roe, K., et al., 2012. West Nile virus-induced disruption of the blood-brain barrier in mice is characterized by the degradation of the junctional complex proteins and increase in multiple matrix metalloproteinases. J. Gen. Virol. 93, 1193–1203. https://doi.org/10.1099/vir.0.040899-0.

Roe, K., Orillo, B., Verma, S. West, 2014. Nile virus-induced cell adhesion molecules on human brain microvascular endothelial cells regulate leukocyte adhesion and modulate permeability of the in vitro blood-brain barrier model. PLoS One 9, e102598. https://doi.org/10.1371/journal.pone.0102598.

Roth-Cross, J.K., Bender, S.J., Weiss, S.R., 2008. Murine coronavirus mouse hepatitis virus is recognized by MDA5 and induces type I interferon in brain macrophages/microglia. J. Virol. 82, 9829–9838. https://doi.org/10.1128/JVI.01199-08.

Santos, R.A., 2014. Angiotensin-(1-7). Hypertension 63, 1138–1147. https://doi.org/10.1161/HYPERTENSIONAHA.113.01274.

Spindler, K.R., Hsu, T.H., 2012. Viral disruption of the blood-brain barrier. Trends Microbiol. 20, 282–290. https://doi.org/10.1016/j.tim.2012.03.009.

Tay, M.Z., Poh, C.M., Renia, L., MacAry, P.A., Ng, L.F.P., 2020. The trinity of COVID-19: immunity, inflammation and intervention. Nat. Rev. Immunol. 20, 363–374. https://doi.org/10.1038/s41577-020-0311-8.

Ulrich, R., et al., 2006. MMP-12, MMP-3, and TIMP-1 are markedly upregulated in chronic demyelinating theiler murine encephalomyelitis. J. Neuropathol. Exp. Neurol. 65, 783–793. https://doi.org/10.1097/01.jnen.0000229990.32795.0d.

Varga, Z., et al., 2020. Endothelial cell infection and endotheliitis in COVID-19. Lancet 395, 1417–1418. https://doi.org/10.1016/S0140-6736(20)30937-5.

Wang, L., Cao, Y., Tang, Q., Liang, G., 2013. Role of the blood-brain barrier in rabies virus infection and protection. Protein Cell 4, 901–903. https://doi.org/10.1007/s13238-013-3918-8.

Wang, Y., Wang, Y., Chen, Y., Qin, Q., 2020. Unique epidemiological and clinical features of the emerging 2019 novel coronavirus pneumonia (COVID-19) implicate special control measures. J. Med. Virol. https://doi.org/10.1002/jmv.25748.

Weksler, B.B., et al., 2005. Blood-brain barrier-specific properties of a human adult brain endothelial cell line. FASEB J. 19, 1872–1874. https://doi.org/10.1096/fj.04-3458fje.

Yang, Y., Rosenberg, G.A., 2011. Blood-brain barrier breakdown in acute and chronic cerebrovascular disease. Stroke 42, 3323–3328. https://doi.org/10.1161/STROKEAHA.110.608257.

Yang, Y., Rosenberg, G.A., 2015. Matrix metalloproteinases as therapeutic targets for stroke. Brain Res. 1623, 30–38. https://doi.org/10.1016/j.brainres.2015.04.024.

Yang, J., et al., 2020. Prevalence of comorbidities and its effects in patients infected with SARS-CoV-2: a systematic review and meta-analysis. Int. J. Infect. Dis. 94, 91–95. https://doi.org/10.1016/j.ijid.2020.03.017.

Zhang, Y., et al., 2020. Coagulopathy and Antiphospholipid antibodies in patients with Covid-19. N. Engl. J. Med. 382, e38. https://doi.org/10.1056/NEJMc2007575.